Polymer 258 (2022) 125315

Contents lists available at ScienceDirect

Polymer

journal homepage: www.elsevier.com/locate/polymer

Stars, combs and bottlebrushes of elastic single-chain nanoparticles

Davide Arena [a], Ester Verde-Sesto [a], José A. Pomposo [a,b,c,*]

[a] Centro de Física de Materiales (CSIC, UPV/EHU) and Materials Physics Center MPC, Paseo Manuel de Lardizábal 5, E-20018, Donostia, Spain
[b] Departamento de Polímeros y Materiales Avanzados: Física, Química y Tecnología, University of the Basque Country (UPV/EHU), PO Box 1072, 20800, Donostia, Spain
[c] IKERBASQUE - Basque Foundation for Science, Plaza de Euskadi 5, 48009, Bilbao, Spain

ARTICLE INFO

Keywords:
Hierarchical self-assembly
Single-chain nanoparticles
Stars
Comb-like polymers
Bottle-brushes

ABSTRACT

Hierarchical self-assembly of structural elements gives rise to superstructures often with outstanding properties when compared to individual elements, as first observed in nature. While folding of individual synthetic chains leads to discrete single-chain nanoparticles (SCNPs) of significant interest for a number of applications, its full potential utility through integration into well-defined superstructures is recently being recognized. Remarkably, SCNPs in good solvent resemble randomly branched polymers with ideal connectivity in a theta-solvent or percolating clusters with screened excluded-volume interactions. Herein we consider the integration of SCNPs into star, comb and bottlebrush topologies and investigate the dimensions of the resulting superstructures under different conditions (good solvent, ideal conformations, 1D- and 2D-confinement in nanopores and nanoslits, anchored to flat surfaces). A detailed comparison of the equilibrium conformational properties of star, comb and bottlebrush polymers composed of elastic SCNPs to those of equivalent topologies based on linear chains is provided. This analysis reveals the effect of hierarchical topology on superstructure dimensions in several relevant environments, as well as how the structural parameters of the SCNPs influence the location of the comb-to-bottlebrush transition as a function of grafting density. The degree of intra-chain cross-linking arises as an additional parameter for controlling the local and global dimensions of stars, combs and bottlebrushes of SCNPs.

1. Introduction

Nature illustrates perfectly how hierarchical self-assembly of individual structural elements gives complex systems with emergent properties (*e.g.,* multimeric proteins, organelles, cells, tissues, whole living organisms) [1]. Formation of superstructures often results in outstanding properties when compared to individual elements. This concept has been also adopted for the association of different synthetic building blocks (molecules [2], macromolecules [3], inorganic nanoparticles [4]) into high-level ordered constructs to obtain materials with unique properties. Moreover, association of elements in synthetic superstructures can be selected to be either dynamic (non-covalent interactions, dynamic covalent bonds) or permanent (covalent bonds).

Single-chain nanoparticles (SCNPs) can be envisioned as simplified synthetic analogues of folded biomacromolecules with potential applications in a number of fields (*e.g.,* catalysis, sensing, drug delivery) [5]. Concerning SCNPs, "folding" denotes the process by which a functionalized polymer chain assumes its final shape or conformation as single-chain nanoparticle through intra-chain interactions (dynamic or permanent) at high dilution. Advances in this thriving field are disclosed in several recent reviews [6–10]. Remarkably, integration of SCNPs into well-defined superstructures is recognized as a promising way to deploy its full potential utility [7]. In this sense, the use of SCNPs as building blocks for construction of high-level ordered constructs is currently highly appealing.

As a first step, one can consider the integration of SCNPs into star, comb and bottlebrush topologies to give permanent superstructures of SCNPs with increasing complexity. However, on passing from individual SCNPs to superstructures of SCNPs, the design space grows notably so guidelines from theoretical approaches to keep synthetic efforts and times feasible become extremely useful. The same problem applies to computer simulations of superstructures involving a huge number of monomers leading to exacerbated computational cost to achieve equilibrated conformations and unbiased results.

In this work, we use the elastic single-chain nanoparticle (ESN) model [11] as an input for a scaling blob theory (stars, bottlebrushes)

* Corresponding author. Centro de Física de Materiales (CSIC, UPV/EHU) and Materials Physics Center MPC, Paseo Manuel de Lardizábal 5, E-20018, Donostia, Spain.
E-mail address: Josetxo.pomposo@ehu.eus (J.A. Pomposo).

https://doi.org/10.1016/j.polymer.2022.125315
Received 23 June 2022; Received in revised form 5 September 2022; Accepted 7 September 2022
Available online 13 September 2022

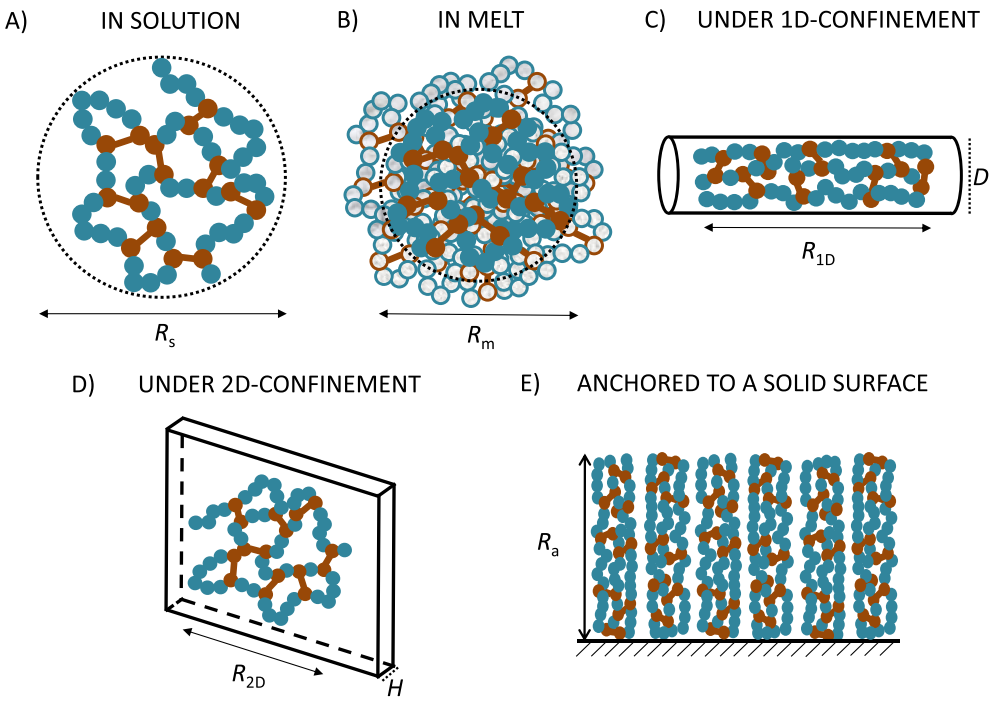

Fig. 1. Schematic illustration of elastic single-chain nanoparticles in the framework of the ESN model [11–13]: A) Size of an isolated elastic single-chain nanoparticle (SCNP) in good solvent at high dilution, R_s. Intra-chain cross-links are denoted by brown color. B) Size of the same SCNP in the ideal state (only ternary excluded-volume interactions involved), R_m. C) Size of a SCNP confined in a long, cylindrical nanopore of diameter D, R_{1D}. D) Size of a SCNP confined in rectangular nanoslit of width H, R_{2D}. E) Size of a brush composed of densely grafted SCNPs on a flat surface, R_a. (For interpretation of the references to color in this figure legend, the reader is referred to the Web version of this article.)

and a Flory free energy approximation (combs) to investigate the equilibrium conformational properties of star, comb and bottlebrush polymers composed of SCNPs in selected cases. The ESN model has been previously employed with success to investigate the conformational properties of neat SCNPs in dilute solution and on surfaces [11], under 1D- and 2D-confinement in nanopores and nanoslits [12], and anchored to flat surfaces [13]. By careful comparison of the properties of stars, combs and bottlebrushes of SCNPs to equivalent constructs of linear chains, insight about the effect of hierarchical topology on superstructure dimensions in several relevant environments will be gained. Significant efforts have been devoted to compare experimental, theoretical and computational results concerning stars, combs and bottlebrushes of linear chains [14–29]. Also worthy of special mention are several theoretical approaches and molecular dynamics simulations based on the analogy of these complex topologies with randomly branched polymers (lattice animals) and percolating clusters [30–34]. Very recently, the conformational properties of complex superstructures such as barbwire bottlebrushes in different environments have been investigated within the framework of the scaling blob approach [35].

The rest of the paper is organized as follows: First, we summarize the main results of the ESN model when applied to SCNPs in different environments (good solvent, ideal conditions, 1D- and 2D-confinement, brushes of SCNPs). Next, we consider the cases of stars, flexible combs and rigid or flexible bottlebrushes composed of SCNPs in equivalent conditions. Finally, we discuss the main results obtained and highlight differences with classical results for stars, combs and bottlebrushes composed of linear chains.

2. The elastic single-chain nanoparticle model

In this section, we first summarize the main results of the elastic single-chain nanoparticle (ESN) model [11] in the case of diluted solutions (good solvent) composed of isolated SCNPs (Fig. 1A) and in the ideal state (*i.e.,* the case of negligible pairwise excluded-volume interactions) (Fig. 1B) which are relevant for our further analysis. Next, we review briefly the predictions of the model for the conformation of an elastic SCNP in a good solvent under confinement [12] (Fig. 1C and D) and the height of a layer of elastic SCNPs densely anchored to a flat surface [12] (Fig. 1E). This overview provides the foundation for tackling the cases of stars, combs, and bottlebrushes of elastic single-chain nanoparticles below. For the sake of simplicity, we set in the model the excluded-volume parameter, the thermal energy, and the effective monomer size (or Kuhn length) to unity. In addition, numerical pre-factors of order unity −that do not change the qualitative features of the results− will be ignored throughout in the following (we use the symbol ≈ to remark this fact). Neutral, flexible chains are only considered. When required for illustrative purposes, a comparison of model predictions to selected experimental data is also carried out.

2.1. Size of elastic single-chain nanoparticles in good solvent conditions at high dilution

The model considers an elastic SCNP containing a total number of monomers n and a fraction of reactive monomers x distributed randomly along the chain. The number of intra-chain cross-links in the SCNP is $nx/2$. A balance between an elastic contribution to the free energy and a contribution arising from intramolecular excluded-volume interactions determines the SCNP size [11]. Hence, the free energy of a SCNP is expressed as:

$$F \approx F_{el} + F_{ev} \quad (1)$$

The elastic contribution to the free energy contains two terms:

$$F_{el} = K R^2 + R^2/R_0^2 \approx A\, x\, R^2 \quad (2)$$

Where $K = Ax$, and A is a constant related to the elasticity of the SCNP [11], R being the SCNP size (*e.g.,* the root mean square radius of gyration normalized to the effective monomer size (or Kuhn length) that we set to unity to treat K and A as dimensionless quantities). The term R^2/R_0^2 in eq. (2) can be neglected when $K > 1/R_0^2 \approx 1/n$, which is often the case. Note that when $x \to 0$ (*i.e.,* $R^2/R_0^2 > K R^2$) we recover the classical result corresponding to uncross-linked linear chains: $F_{el} \approx R^2/R_0^2$. Although the elastic free energy (and hence A) could be obtained from the fundamental statistical mechanics of SCNPs in the presence of excluded volume interactions, attaining an analytical solution is still a formidable problem [36,37]. Consequently, we treat A as a model parameter that can be extracted from available experimental data (see below).

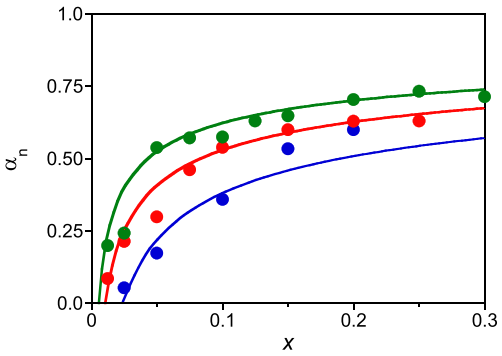

Fig. 2. Comparison of ESN model predictions (continuous lines) and experimental data of poly(styrene) (PS) SCNPs in good solvent conditions [40] corresponding to samples of different polymerization degree, *DP* (green solid circles: *DP* = 1880; red solid circles: *DP* = 980, and blue solid circles: *DP* = 410). Continuous lines calculated from eq. (7) with $A = 2$ and $n \approx DP/20$ (see text for details). (For interpretation of the references to color in this figure legend, the reader is referred to the Web version of this article.)

The excluded-volume contribution to the free energy in the case of a good solvent is [39]:

$$F_{ev} \approx n^{2} / R^{3} \tag{3}$$

Minimization of eq. (1) with respect to R in terms of eqs. (2) and (3) gives the equilibrium average size of the SCNP in good solvent conditions (denoted as R_s, see Fig. 1A):

$$R_s \approx K^{-1/5} n^{2/5} \tag{4}$$

Remarkably, the mass scaling of SCNPs in good solvent is close to that estimated for randomly branched polymers with ideal connectivity in a theta-solvent and percolating clusters with screened excluded-volume interactions [30,31,34].

It is worth of mentioning that the ESN model is not equivalent to gel models like Flory-Rehner theory or de Gennes'c*-theorem providing the equilibrium degree of swelling of a gel in a good solvent as a function of strand length [39]. Instead, the ESN model gives the average global size of an isolated SCNP in good solvent as a function of its elasticity constant A, the fraction of intramolecular cross-links x, and the total number of monomers n. Remarkably, the ESN model can be easily combined with scaling arguments to estimate the SCNP domain size at local length scale as described in detail in ref. [38].

The shrinking factor α_R –defined as the ratio of R_s to that of a linear chain of n monomers in good solvent conditions (denoted as R_l, where $R_l \approx n^{\nu F}$ and $\nu_F \approx 3/5$ [39])– is just:

$$\alpha_R = R_s / R_l \approx (K n)^{-1/5} \tag{5}$$

For comparison to available experimental data of percent reduction in (apparent) molecular weight upon SCNP formation, it is instructive to introduce the apparent value of n associated to an elastic SCNP of size R_s as if it was a linear chain in good solvent ($n_{app} \approx R_s^{5/3}$). In terms of the model, n_{app} is given by:

$$n_{app} \approx K^{-1/3} n^{2/3} \tag{6}$$

and to define the corresponding shrinking factor related to n_{app} such as:

$$\alpha_n = 1 - (n_{app} / n) \approx 1 - (A\, x\, n)^{-1/3} \tag{7}$$

As illustrated in Fig. 2, the model reproduces reasonably well the observed experimental data of poly(styrene) (PS) SCNPs [40] with a value of $A = 2$ for $n = 93$ (green line), $n = 48$ (red line) and $n = 21$ (blue line). The selected values of n, which correspond to $n \approx DP/20$ where *DP* is the experimental polymerization degree determined by size exclusion chromatography (SEC) using PS standards, provided a good estimation of the size of the PS-SCNPs in good solvent at high dilution *via* eq. (4) (data not shown).

2.2. Ideal size of elastic single-chain nanoparticles

To estimate the ideal size of an elastic SCNP (*i.e.,* in a theta solvent, in the melt) we assume complete screening of binary excluded-volume interactions such as only ternary interactions will contribute to F_{ev} [39]. Hence, we can write:

$$F_{ev} \approx n^{3} / R^{6} \tag{8}$$

Minimization of the free energy according to eq. (1) with respect to R in terms of eqs. (2) and (8) gives the ideal size of the elastic SCNP (denoted as R_m, see Fig. 1B):

$$R_m \approx K^{-1/8} n^{3/8} \tag{9}$$

Note that the scaling exponent $\nu = 3/8 = 0.375$ in eq. (9) is close to the scaling exponent observed for SCNPs under crowding in both molecular dynamics simulations and experiments ($\nu \approx 0.37$) [41]. The shrinking factor α_M –defined as the ratio of R_m to R_s (eq. (4))– is:

$$\alpha_M = R_m / R_s \approx (K^{3} / n)^{1/40} \tag{10}$$

Accurate experimental data of R_s and R_m as determined *e.g.* from small angle neutron scattering (SANS) measurements allow one to estimate (effective) values of K and n from eqs. (9) and (10). As an example, we obtain $K \approx 0.53$ and $n \approx 88$ for PMMA-based SCNPs of 92 kDa in molar mass based on the reported values [42] of R_s (SANS) = 6.8 and R_m (SANS) = 5.8 (dimensionless by normalization to the Kuhn segment length taken as 1 nm).

2.3. Size of elastic single-chain nanoparticles in good solvent under confinement

The size of a SCNP under 1D-confinement in long, cylindrical nanopores or 2D-confinement in rectangular nanoslits is altered when compared to its equilibrium size without dimensional constraints, R_s.

1D-Confinement: In a cylindrical nanopore of diameter $D \ll R_s$ an elastic SCNP in good solvent conditions will be confined to a volume proportional to $D^2 R_{1D}$, where R_{1D} is the SCNP size along the channel axis (Fig. 1C). According to eq. (1), the free energy of the 1D-confined SCNP can be expressed as [12]:

$$F \approx K R^{2} + n^{2} / (D^{2} R) \tag{11}$$

Minimization of eq. (11) with respect to R provides the equilibrium configuration of the SCNP under 1D-confinement:

$$R_{1D} \approx K^{-1/3} (n / D)^{2/3} \tag{12}$$

As expected, in the limit $D = R_{1D} = R_s$ eq. (12) becomes eq. (4). The minimum nanopore diameter in which the SCNP can be confined, D_{min}, can be determined by combining the highest possible packing of the isolated SCNP inside the pore: $\varphi \approx n/(D_{min}^{2} R_{1D}) = 1$ and eq. (12), so we obtain:

$$D_{min} \approx (K n)^{1/4} \tag{13}$$

Note that D_{min} depends on both the elasticity parameter K and n. Hence, eq. (12) is valid in the range: $D_{min} \leq D \leq R_s$.

2D-Confinement: In a rectangular nanoslit of width $H \ll R_s$ an elastic SCNP in good solvent conditions will be confined to a volume proportional to HR_{2D}^2, where R_{2D} is the lateral size of the SCNP in the slit (Fig. 1D). Under such conditions, the free energy of the 2D-confined SCNP becomes [12]:

$$F \approx K R^{2} + n^{2} / (H R^{2}) \tag{14}$$

Minimization of eq. (14) with respect to R provides the equilibrium configuration of the SCNP under 2D-confinement:

Table 1
Comparison of Conformational Properties of Elastic Single-Chain Nanoparticles (SCNPs) *vs.* Flexible Linear Polymers (LPs)[a].

Conditions	Size	
	SCNPs	LPs
Good solvent, high dilution	$R_s \approx K^{-1/5} n^{2/5}$	$R_s \approx n^{3/5}$
Theta solvent, high dilution/melt state	$R_m \approx K^{-1/8} n^{3/8}$	$R_m \approx n^{1/2}$
1D-confinement, good solvent	$R_{1D} \approx K^{-1/3} n^{2/3} D^{-2/3}$	$R_{1D} \approx n D^{-2/3}$
2D-confinement, good solvent	$R_{2D} \approx K^{-1/4} n^{1/2} H^{-1/4}$	$R_{2D} \approx n^{3/4} H^{-1/4}$
Dense brush, good solvent	$R_a \approx K^{-1/3} n^{2/3} \sigma^{1/3}$	$R_a \approx n \sigma^{1/3}$

[a] K = SCNP elasticity parameter; n = number of monomers; D = nanopore diameter; H = nanoslit width; σ = brush grafting density.

$$R_{2D} \approx (K H)^{-1/4} n^{1/2} \quad (15)$$

Note that in the limit $H = R_{2D} = R_s$ eq. (15) becomes eq. (4). The minimum nanoslit width in which the SCNP can be confined, H_{min}, is determined from highest possible packing of the isolated SCNP inside the slit: $\varphi \approx n/(H_{min} R_{2D}^2) = 1$. By taking into account eq. (15) we obtain:

$$H_{min} \approx K \quad (16)$$

In this case, H_{min} is determined exclusively by the elasticity parameter K. Eq. (15) is valid in the range: $H_{min} \leq H \leq R_s$.

2.4. Size of elastic single-chain nanoparticles on surfaces immersed in a good solvent

A schematic illustration of a brush composed of densely grafted elastic SCNPs on a flat surface immersed in a good solvent is depicted in Fig. 1E. We consider that the average distance between SCNPs is d and hence the grafting density is $\sigma = 1/d$ [2]. Each elastic SCNP in the brush will be confined to a volume proportional to $d^2 R_a$, where R_a is the SCNP size in the direction perpendicular to the surface. The free energy of the SCNP in the brush can be expressed as [13]:

$$F \approx K R^2 + n^2 \sigma / R \quad (17)$$

Minimization of eq. (17) with respect to R gives the equilibrium size of the SCNP anchored to the surface:

$$R_a \approx (\sigma / K)^{1/3} n^{2/3} \quad (18)$$

In the limit $\sigma = 1/R_a^2 = 1/R_s^2$ eq. (18) becomes eq. (4). The maximum grafting density of elastic SCNPs in the brush, σ_{max}, is determined by combining the highest possible packing in the brush, $\varphi \approx n \sigma_{max}/R_a = 1$, and eq. (18). Hence:

$$\sigma_{max} \approx (K n)^{-1/2} \quad (19)$$

As a proof of consistency, we obtain identical result (eq. (19)) starting from the free energy of a SCNP in the brush with screening of binary excluded-volume interactions ($F = K R^2 + n^3 \sigma^2/R^2$) and the maximum packing condition ($\varphi = 1$). It is worth mentioning that the maximum height of a brush of elastic SCNPs at highest possible packing is just: $R_a(\sigma_{max}) = (n/K)^{1/2}$.

We summarize in Table 1 the conformational properties of elastic SCNPs in different conditions according to the ESN model compared to those of flexible linear polymers, whereas the differences in the scaling exponent for n can be appreciated in Fig. 3A. In the case of SCNPs, the scaling exponent for K in several environments is shown in Fig. 3B.

3. Star polymers of elastic single-chain nanoparticles

Let us consider the case of a star polymer comprising f arms connected to a core in which each arm is an elastic single-chain nanoparticle

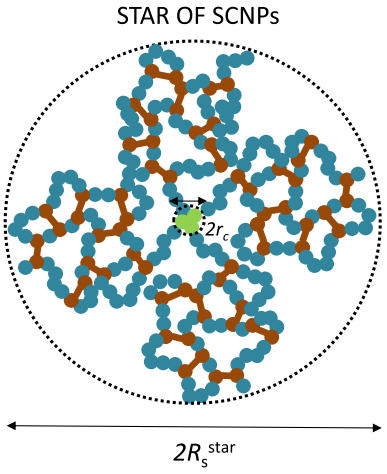

Fig. 4. Schematic illustration of a polymer star of size R_s^{star} composed of elastic single-chain nanoparticles in good solvent conditions (number of arms: $f = 4$). We consider the case in which the size of the core (r_c) is small when compared to the global size of the star ($r_c \ll R_s^{star}$).

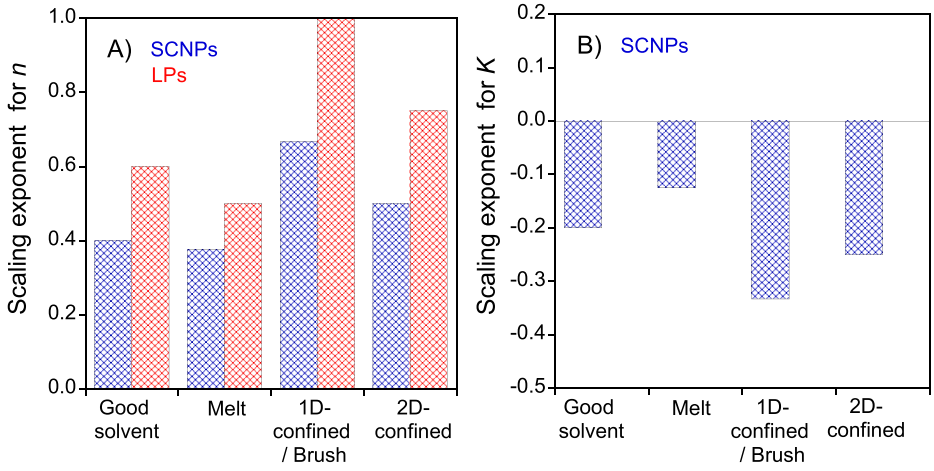

Fig. 3. A) Comparison of the scaling exponent for n corresponding to the conformational properties under different conditions (see Table 1) of elastic SCNPs (blue grid bars) vs. flexible linear polymers (red grid bars). B) Scaling exponent for K (see Table 1) of elastic SCNPs in different conditions. (For interpretation of the references to color in this figure legend, the reader is referred to the Web version of this article.)

with n segments (see Fig. 4). In the following, we will address the case in which the size of the core (r_c) is small when compared to the size of the star (R_s^{star}), *i.e.* $r_c \ll R_s^{star}$.

3.1. Size of a star of elastic single-chain nanoparticles in good solvent conditions at high dilution

We will combine the elastic single-chain nanoparticle (ESN) model [11] with the Daoud-Cotton (DC) model [17] to determine the size of a star polymer comprising f arms connected to a core in which each arm is an elastic single-chain nanoparticle with n segments. The number of intra-chain cross-links in each SCNP is given by $nx/2$, x being the fraction of reactive monomers of the SCNP. We will assume that the size of the core (r_c) is negligible when compared to the size of the star of SCNPs (R_s^{star}). We consider the star immersed in a good solvent at high dilution conditions.

According to the DC model, we can describe the interior of the star of SCNPs as an array of concentric shells of closely packed blobs [17]. From geometrical considerations, the blob size (ξ) at a distance r from the star center is:

$$\xi(r) \approx r / f^{1/2} \tag{20}$$

In the external part of the star, inside each blob containing g monomers (good solvent conditions) we can assume according to the ESN model [11]:

$$\xi(r) \approx K^{-1/5}\, g^{2/5}(r) \tag{21}$$

Similar approaches to estimate the blob size have been followed for the case of other complex architectures such as randomly branched polymers in confined spaces [43]. By combining eqs. (20) and (21) we obtain an expression for the number of monomers per blob as a function of r:

$$g(r) \approx r^{5/2} f^{-5/4} K^{1/2} \tag{22}$$

The expansion parameter of the blobs is:

$$\alpha_b(r) \approx \xi(r) / \xi_0(r) \tag{23}$$

Where

$$\xi_0(r) \approx K^{-1/8}\, g^{3/8}(r) \tag{24}$$

is the size of an ideal blob in which the concentration is high enough to screen out binary excluded-volume interactions. From eqs. (21), (23) and (24) we obtain:

$$\alpha_b(r) \approx r^{1/16} f^{-1/32} K^{-1/16} \tag{25}$$

The segment concentration profile as a function of r can be determined from [17]:

$$\varphi(r) \approx g(r) / \xi^3(r) \tag{26}$$

so by combining eqs. (21), (22) and (26) we obtain:

$$\varphi(r) \approx f^{1/4} (K / r)^{1/2} \tag{27}$$

It is worth of mention that eqs. (21), (22), (25) and (27) are valid until $\alpha_b(r) = 1$; *i.e.,* until the blob size (eq. (22)) reaches the size of an ideal blob (eq. (24)). This will take place at a radial distance r_1 from the star center ($r = 0$) given by:

$$r_1 \approx K f^{1/2} \tag{28}$$

Since the segment concentration profile at r_1 is $\varphi(r_1) \approx 1$ (*i.e.,* both ξ and g are of order of unity), hence, at r_1 we actually reach the core of the star (*i.e.,* $r_c = r_1$).

An expression for the size of a star of elastic SCNPs in good solvent at high dilution (R_s^{star}) can be obtained from the segment concentration profile through [17]:

$$nf = \int_0^{R_s^{star}} \varphi(r) r^2 dr \tag{29}$$

by assuming $r_1/R_s^{star} \ll 1$. From eqs. (27) and (29), we obtain:

$$R_s^{star} \approx f^{3/10} K^{-1/5} n^{2/5} = f^{3/10} R_s \tag{30}$$

Hence, the number of arms f, the number of monomers per arm n and the elasticity parameter K –that is tunable through the fraction of reactive monomers x ($K \approx Ax$)– control the size of an isolated star of SCNPs in a good solvent. As expected, eq. (30) reduces to eq. (4) for $f = 1$. Due to the cooperative effect of interbranch repulsion, each SCNP arm in the star is elongated when compared to an individual, equivalent SCNP in solution. The elongation degree depends on the number of SCNPs in the star according to: $R_s^{star}/R_s \approx f^{3/10}$. From eqs. (28) and (30), the ratio of the size of the core to the size of the star is:

$$r_1 / R_s^{star} \approx f^{1/5} K^{6/5} n^{-2/5} \tag{31}$$

As an illustrative example, for $f = 5$, $K = 0.5$ and $n = 100$ we obtain $R_s^{star}/R_s = 1.62$ and $r_1/R_s^{star} = 0.095$ from eqs. (30) and (31), respectively.

It is instructive, at this stage, to determine R_s^{star} from the mean-field expression of the free energy (eq. (1)) for a star composed of SCNPs in good solvent at high dilution:

$$F \approx f K R^2 + (f n)^2 / R^3 \tag{32}$$

By minimizing eq. (32) with respect to R we obtain:

$$R_s^{star} \approx f^{1/5} K^{-1/5} n^{2/5} = f^{1/5} R_s \tag{33}$$

Eq. (33) is similar to eq. (30) but with a scaling exponent of the dependence of R_s^{star} on f that is slightly lower. The smaller exponent can be attributed to the failure of the mean-field model of a star of SCNPs to capture appropriately the effect of local fluctuations and inter-branch repulsion, opposite to the scaling blob model [44]. For $f = 5$, $K = 0.5$ and $n = 100$ we obtain $R_s^{star} = 11.75$ from eq. (30), and $R_s^{star} = 10.0$ from eq. (33). To be consistent with the scaling blob model, a correction can be introduced in eq. (32) such as:

$$F \approx f K R^2 + f^{1/2} (f n)^2 / R^3 \tag{34}$$

Hence, factor $f^{1/2}$ in the r.h.s. of eq. (34) accounts for local fluctuations and inter-branch repulsion effects [44] that increase the excluded-volume contribution to the free energy (F_{ev}). Minimization of eq. (34) with respected to R provides the scaling blob model expression, eq. (30). We will return to eq. (34) below to obtain the size of a star of SCNPs in good solvent conditions under confinement and the height of a dense brush of stars of SCNPs.

The free energy per arm in the scaling blob model can be estimated from [17]:

$$F_s^{arm} = \int_{r_1}^{r_1+R_s^{star}} \frac{dr}{\xi} = f^{1/2} \int_{r_1}^{r_1+R_s^{star}} \frac{dr}{r} \tag{35}$$

where dr/ξ counts the number of blobs, and each blob is assumed to contribute with k_BT units (recall we assume $k_BT \equiv 1$). We obtain:

$$F_s^{arm} \approx f^{1/2} ln\left[\left(\frac{R_s^{star}}{r_1}\right) + 1\right] = f^{1/2} ln\left[f^{-1/5} K^{-6/5} n^{2/5} + 1\right] \tag{36}$$

3.2. Ideal size of a star of elastic single-chain nanoparticles

The ideal size of a star of SCNPs (*i.e.,* negligible pairwise excluded-volume interactions) [39] can be derived by taking into account that for every blob of the star: $\alpha_b(r) \approx 1$. Thus, the blob size at a distance r

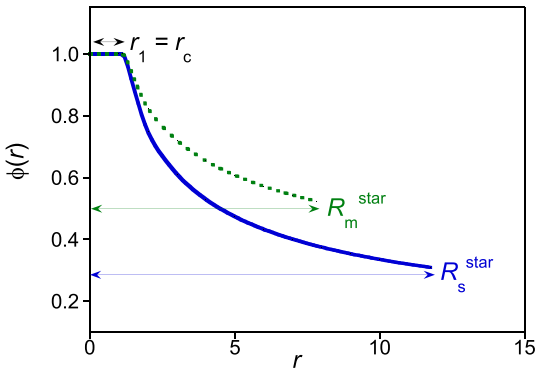

Fig. 5. Segment concentration profile (φ) as a function of the distance from the center (r) of a star of SCNPs ($f = 5$, $K = 0.5$, $n = 100$) in good solvent at high dilution (continuous blue line) and in the ideal state (dotted green line) according to eq. (27) and eq. (39), respectively. (For interpretation of the references to color in this figure legend, the reader is referred to the Web version of this article.)

from the star center is now given by:

$$\xi_0(r) \approx r / f^{1/2} \tag{37}$$

and eq. (24). Hence, the number of monomers per blob and the segment concentration profile as a function of r become respectively:

$$g(r) \approx r^{8/3} f^{-4/3} K^{1/3} \tag{38}$$

and

$$\varphi(r) \approx f^{1/6} (K / r)^{1/3} \tag{39}$$

The core of the star will be located at a distance r_1 at which $\varphi(r_1) \approx 1$. From eq. (39) we obtain: $r_1 \approx K f^{1/2}$, a result identical to that obtained for a star of SCNPs in good solvent conditions (eq. (28)). The ideal size of a star of SCNPs (R_m^{star}) as obtained through integration of the segment concentration profile is:

$$R_m^{star} \approx f^{5/16} K^{-1/8} n^{3/8} = f^{5/16} R_m \tag{40}$$

and the ratio of the size of the core to the ideal size of the star is:

$$r_1 / R_m^{star} \approx f^{3/16} K^{9/8} n^{-3/8} \tag{41}$$

Fig. 5 shows a comparison of the segment concentration profile as a function of r of a star of SCNPs ($f = 5$, $K = 0.5$, $n = 100$) in good solvent at high dilution and in the ideal state (*i.e.,* in the case of negligible pairwise excluded-volume interactions). Also illustrated in Fig. 5 are the size of the core ($r_c = r_1$), and the global dimensions of the star in both conditions (R_s^{star} and R_m^{star}, respectively).

An estimation of R_m^{star} from the mean-field expression of the free energy (eq. (1)) gives:

$$R_m^{star} \approx f^{1/4} K^{-1/8} n^{3/8} = f^{1/4} R_m \tag{42}$$

which differs from eq. (40) only in the value of the scaling exponent of R_m^{star} on f. Eq. (40) from the scaling blob model that takes local effects into account [44] is presumably more accurate than the mean-field expression, eq. (42).

According to the scaling blob model, the free energy per arm of an ideal star of SCNPs is:

$$F_m^{arm} \approx f^{1/2} ln\left[\left(\frac{R_m^{star}}{r_1}\right) + 1\right] = f^{1/2} ln\left[f^{-5/16} K^{-9/8} n^{3/8} + 1\right] \tag{43}$$

3.3. Size of a star of elastic single-chain nanoparticles in good solvent under confinement

1D-Confinement: Let us assume that a star of elastic SCNPs is confined in good solvent conditions in a cylindrical nanopore of diameter $D \ll R_s^{star}$. The volume occupied by the star will be proportional to $D^2 R_{1D}^{star}$, where R_{1D}^{star} is the size along the channel axis. From eq. (34), the free energy of a star of SCNPs under 1D-confinement can be expressed as:

$$F \approx f K R^2 + f^{1/2} (f n)^2 / (D^2 R) \tag{44}$$

Minimization of eq. (44) with respect to R provides the equilibrium configuration of the star under 1D-confinement:

$$R_{1D}^{star} \approx f^{1/2} K^{-1/3} (n / D)^{2/3} = f^{1/2} R_{1D} \tag{45}$$

Note that for $f = 1$ we recover eq. (12), as it must. The minimum nanopore diameter in which the star of SCNPs can be confined, D_{min}^{star}, is obtained from the condition: $\varphi \approx n/[(D_{min}^{star})^2 R_{1D}^{star}] = 1$ and eq. (45), such as:

$$D_{min}^{star} \approx f^{-3/8} (K n)^{1/4} = f^{-3/8} D_{min} \tag{46}$$

Note that D_{min}^{star} depends on f, in addition to K and n. For $f = 1$, eq. (46) becomes eq. (13).

2D-Confinement: A star of SCNPs placed in a rectangular nanoslit of width $H \ll R_s^{star}$ will be confined to a volume proportional to $H(R_{2D}^{star})^2$, where R_{2D}^{star} is the lateral size of the SCNP in the slit. Hence, based on eq. (34), the free energy of the star under 2D-confinement is given by:

$$F \approx f K R^2 + f^{1/2} (f n)^2 / (H R^2) \tag{47}$$

Minimization of eq. (47) with respect to R provides the equilibrium configuration of the star under 2D-confinement:

$$R_{2D}^{star} \approx f^{3/8} (K H)^{-1/4} n^{1/2} = f^{3/8} R_{2D} \tag{48}$$

As expected, eq. (48) becomes eq. (15) for $f = 1$. The minimum nanoslit width in which the star of SCNPs can be confined, H_{min}^{star}, is determined from highest possible packing of the isolated SCNP inside the slit: $\varphi \approx n/[H_{min}^{star} (R_{2D}^{star})^2] = 1$ and eq. (48), so:

$$H_{min}^{star} \approx f^{-3/2} K = f^{-3/2} H_{min} \tag{49}$$

Note that H_{min}^{star} depends on both f and K.

3.4. Height of a brush of stars of elastic single-chain nanoparticles anchored to a surface immersed in a good solvent

We consider here the most relevant case of a brush of stars with f SCNP arms on a flat surface immersed in a good solvent in which each star is anchored to the surface by the external part of a single arm. The average distance between anchored arms is d and hence the grafting density is $\sigma = 1/d^2$. Accordingly, each star of elastic SCNPs in the brush will be confined to a volume proportional to $d^2 R_a^{star}$, where R_a^{star} is the size of the star in the direction perpendicular to the surface (*i.e.,* the average brush height). According to eq. (34), the free energy of the star in the brush can be expressed as:

$$F \approx f K R^2 + f^{1/2} (f n)^2 \sigma / R \tag{50}$$

Minimization of eq. (50) with respect to R gives the equilibrium height of the brush:

$$R_a^{star} \approx f^{1/2} (\sigma / K)^{1/3} n^{2/3} = f^{1/2} R_a \tag{51}$$

For $f = 1$, eq. (51) becomes eq. (18). The maximum grafting density of stars in the brush, σ_{max}^{star}, is determined by combining the highest possible packing in the brush, $\varphi \approx n\, \sigma_{max}^{star} / R_a^{star} = 1$, and eq. (51). Hence:

$$\sigma_{max}^{star} \approx f^{3/4} (K n)^{-1/2} = f^{3/4} \sigma_{max} \tag{52}$$

Then, the maximum height of a brush of stars composed of SCNPs at highest possible packing is: $R_a^{star} (\sigma_{max}^{star}) = f^{3/4} R_a(\sigma_{max})$. Notice that eq. (52) depends on f, K and n, and it becomes eq. (19) for $f = 1$.

Table 2 summarizes the scaling laws obtained for stars of SCNPs in

Table 2
Comparison of Conformational Properties of Star Polymers Composed of Elastic Single-Chain Nanoparticles (SCNPs) *vs.* Stars of Linear Polymers (LPs)[a].

Conditions	Size	
	Stars of SCNPs	Stars of LPs
Good solvent, high dilution	$R_s^{star} \approx f^{3/10} K^{-1/5} n^{2/5}$	$R_s^{star} \approx f^{1/5} n^{3/5}$
Ideal state, negligible pairwise excluded-volume interactions	$R_m^{star} \approx f^{5/16} K^{-1/8} n^{3/8}$	$R_m^{star} \approx f^{1/4} n^{1/2}$
1D-confinement, good solvent	$R_{1D}^{star} \approx f^{1/2} K^{-1/3} n^{2/3} D^{-2/3}$	$R_{1D}^{star} \approx f^{1/3} n D^{-2/3}$
2D-confinement, good solvent	$R_{2D}^{star} \approx f^{3/8} K^{-1/4} n^{1/2} H^{-1/4}$	$R_{2D}^{star} \approx f^{1/4} n^{3/4} H^{-1/4}$
Dense brush, good solvent	$R_a^{star} \approx f^{1/2} K^{-1/3} n^{2/3} \sigma^{1/3}$	$R_a^{star} \approx f^{1/3} n \sigma^{1/3}$

[a] f = number of arms in the star polymer; K = SCNP elasticity parameter; n = number of monomers per arm; D = nanopore diameter; H = nanoslit width; σ = brush grafting density.

this work and those reported for stars of linear polymers [17,45] (LPs) whereas a visual comparison of the scaling exponents for f and n in both cases is shown in Fig. 6.

4. Comb polymers of elastic single-chain nanoparticles

Fig. 7 depicts the conformation of a comb polymer composed of elastic SCNPs in good solvent conditions. The main chain is taken as non-charged and flexible. In the comb polymer, SCNPs are attached regularly every m monomer units along the main chain that has a total number of monomers M. Hence, the grafting density is $z = 1/m$. Each SCNP contains n monomers and $nx/2$ intramolecular cross-links, x being the fraction of reactive monomers. For simplicity, we consider the monomers of the main chain and those of the side SCNPs to possess the same characteristics. The total number of monomers in the comb polymer is $T = M + (M/m)\, n = M\,(1 + z\, n)$. Depending on the grafting density, we distinguish between comb polymers of SCNPs (*i.e.,* $z \ll 1$) and brush polymers of SCNPs (*i.e.,* $z \to 1$).

4.1. Size of a comb polymer of elastic single-chain nanoparticles in good solvent conditions at high dilution

The conformation of comb polymers with low grafting density ($z \ll 1$) is expected to be only slightly modified when compared to that a linear chain [28]. The free energy of a comb polymer containing branches of size R_s can be expressed, to a first approximation, as [29]:

$$F \approx R^2/M + M^2/R^3 + R_s^3\,(z\,M)^2/R^3 \tag{53}$$

where the effect of the branches is taken into account through the last term in eq. (53). Minimization of eq. (53) with respect to R gives an expression for the global size of the comb polymer in good solvent conditions at high dilution, R_s^{comb}:

$$R_s^{comb} \approx M^{3/5}\,(1 + z^2\, R_s^3)^{1/5} \tag{54}$$

Remarkably, for comb polymers of linear branches with $z^2 R_s^3 > 1$ eq. (54) reduces to $R_s^{comb} \approx M^{3/5}\,(n^{9/25}/m^{2/5})$ which is a result very similar to that obtained by Rouault and Borisov [27] from a scaling blob model (*i.e.,* $R_s^{comb} \approx M^{3/5}\,(n/m)^{9/25}$).

For a comb polymer of elastic SCNPs ($z \ll 1$) we can assume that the size of a side SCNP is not disturbed by the presence of the other SCNPs attached to the main chain so it can be estimated directly from: $R_s \approx K^{-1/5} n^{2/5}$ (eq. (4)). Hence, from eq. (54) we obtain:

$$R_s^{comb} \approx M^{3/5}\,(1 + z^2\, K^{-3/5}\, n^{6/5})^{1/5} \tag{55}$$

Note that if $n \to 0$ or $z \to 0$ eq. (55) becomes:

$$R_s^{comb} \approx M^{3/5} \tag{56}$$

which is the size expected for the comb main chain without SCNP pendants. A comparison of eq. (55) and eq. (56) for a comb polymer of SCNPs with $m = 25$, $n = 50$ and $K = 0.5$ as a function of M is provided in Fig. 8. We will determine below the critical value of grafting density at which eq. (55) lacks validity (see eq. (86)).

4.2. Ideal size of a comb polymer of elastic single-chain nanoparticles

The ideal size of a comb polymer of SCNPs (*i.e.,* low grafting density, $z \ll 1$) can be estimated from:

$$F \approx R^2/M + M^3/R^6 + R_m^3\,(z\,M)^3/R^6 \tag{57}$$

where R_m is given by eq. (9). Minimization of eq. (57) with respect to R gives an expression for the ideal size of a comb polymer of SCNPs, R_m^{comb}:

$$R_m^{comb} \approx M^{1/2}\,(1 + z^3\, R_m^3)^{1/8} = M^{1/2}\,(1 + z^3\, K^{-3/8}\, n^{9/8})^{1/8} \tag{58}$$

The grafting density at which eq. (58) lacks validity will be provided below (see eq. (93)).

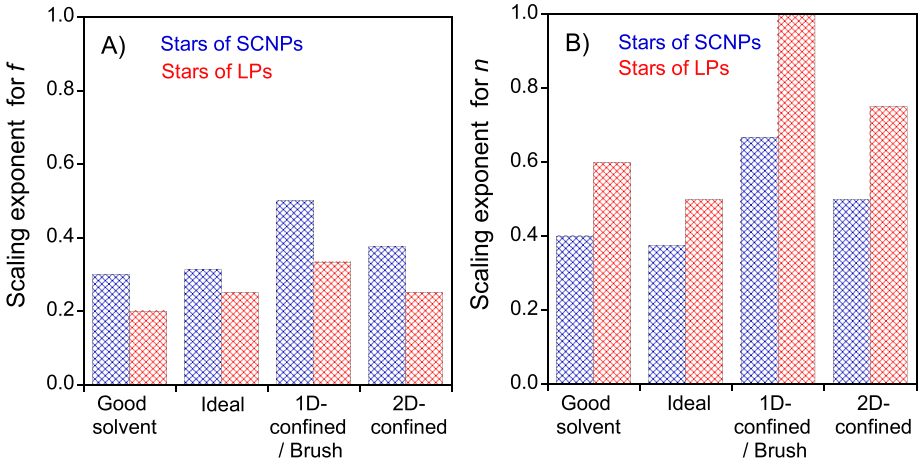

Fig. 6. Comparison of the scaling exponents for f (A) and n (B) corresponding to the conformational properties under different conditions (see Table 2) of stars composed of elastic SCNPs (blue grid bars) vs. stars composed of linear polymers (red grid bars). (For interpretation of the references to color in this figure legend, the reader is referred to the Web version of this article.)

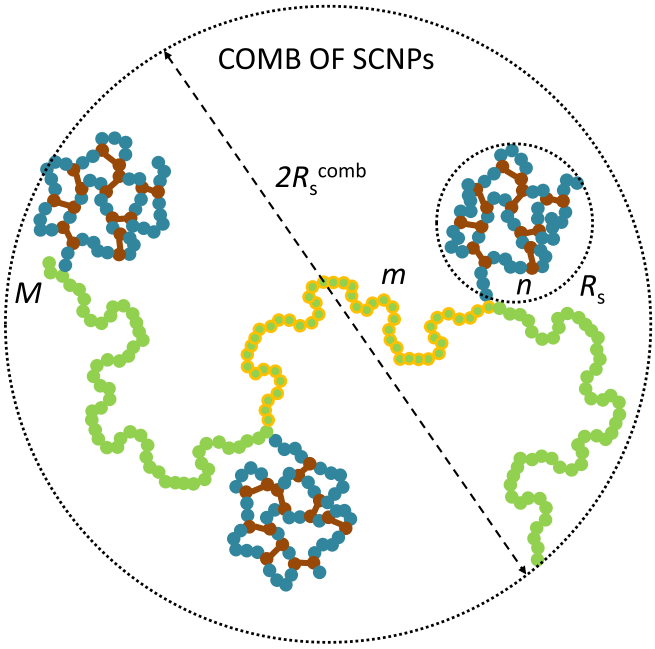

Fig. 7. Schematic illustration of a comb polymer composed of elastic single-chain nanoparticles in good solvent conditions. SCNPs of size R_s are spaced regularly along the main chain composed of M monomers. The average number of monomers between grafting points along the main chain is m and each SCNP contains n monomers. The grafting density is $z = 1/m \ll 1$.

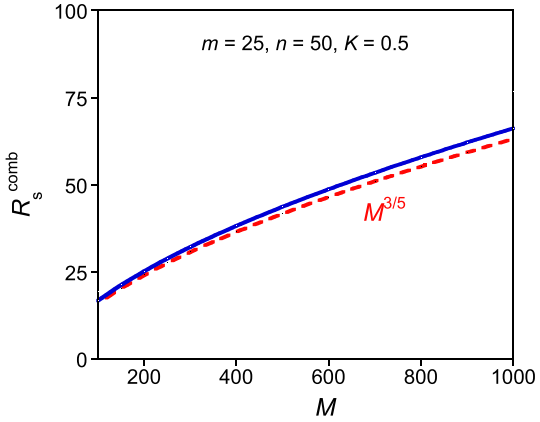

Fig. 8. Size of a comb polymer of SCNPs in good solvent conditions at high dilution (R_s^{comb}) as a function of the total number of monomers of the main chain (M) according to: $R_s^{comb} \approx M^{3/5}\ [1 + z^2\ R_s^3]^{\ 1/5}$ (continuous blue line, eq. (54)) and estimated from the limiting expression: $R_s^{comb} \approx M^{3/5}$ (dotted red line, eq. (56)). R_s is the size of an elastic SCNP with elasticity parameter K and n monomers (see eq. (4)), $z = 1/m$ is the grafting density, and m is the number of monomers between grafting points along the main chain. (For interpretation of the references to color in this figure legend, the reader is referred to the Web version of this article.)

4.3. Size of a comb polymer of elastic single-chain nanoparticles in good solvent under confinement

1D-Confinement: In a cylindrical nanopore of diameter $R_s \ll D \ll R_s^{comb}$, the volume occupied by a comb polymer of elastic SCNPs (each SCNP of size R_s) confined in good solvent conditions is proportional to $D^2 R_{1D}^{comb}$, where R_{1D}^{comb} is the size along the channel axis. From eq. (53), the free energy of the comb polymer in these conditions can be expressed as:

Table 3
Conformational Properties of Comb Polymers (Low Grafting Density) Composed of Elastic SCNPs *vs.* Combs of LPs[a].

Conditions	Size	
	Combs of SCNPs	Combs of LPs
Good solvent, high dilution	$R_s^{comb} \approx M^{3/5}(1 + z^2K^{-3/5}n^{6/5})^{1/5}$	$R_s^{comb} \approx M^{3/5}(1 + z^2n^{9/5})^{1/5}$
Ideal state	$R_m^{comb} \approx M^{1/2}(1 + z^3K^{-3/8}n^{9/8})^{1/8}$	$R_m^{comb} \approx M^{1/2}(1 + z^3n^{3/2})^{1/8}$
1D-confinement, good solvent	$R_{1D}^{comb} \approx M[(1 + z^2\,K^{-3/5}n^{6/5})/D^2]^{1/3}$	$R_{1D}^{comb} \approx M[(1 + z^2\,n^{9/5})/D^2]^{1/3}$
2D-confinement, good solvent	$R_{2D}^{comb} \approx M^{3/4}[(1 + z^2K^{-3/5}n^{6/5})/H]^{1/4}$	$R_{2D}^{comb} \approx M^{3/4}[(1 + z^2n^{9/5})/H]^{1/4}$
Brush, good solvent	$R_a^{comb} \approx M[(1+ z^2K^{-3/5}n^{6/5})\sigma]^{1/3}$	$R_a^{comb} \approx M[(1+ z^2n^{9/5})\sigma]^{1/3}$

[a] M = number of monomers in the comb main chain; z = grafting density of the comb main chain ($z = 1/m \ll 1$); K = SCNP elasticity parameter; n = number of monomers per branch; D = nanopore diameter; H = nanoslit width; σ = grafting density of the brush.

$$F \approx R^{\,2}/M + M^{\,2}\,(1 + z^{\,2}\,R_s^{\,3})\,/\,(D^{\,2}\,R) \tag{59}$$

Minimization of eq. (59) with respect to R provides the equilibrium configuration of the comb polymer of SCNPs under 1D-confinement ($R_s \ll D \ll R_s^{comb}$):

$$R_{1D}^{comb} \approx M\,[(1 + z^{\,2}\,R_s^{\,3})\,/\,D^{\,2}\,]^{\,1/3} = M\,[\,(1 + z^{\,2}\,K^{\,-3/5}\,n^{\,6/5})\,/\,D^{\,2}\,]^{\,1/3} \tag{60}$$

2D-Confinement: A comb polymer of SCNPs (each SCNP of size R_s) placed in a rectangular nanoslit of width $R_s \ll H \ll R_s^{star}$ will be confined to a volume proportional to $H(R_{2D}^{comb})^2$, where R_{2D}^{comb} is the lateral size of the comb in the slit. Hence, based on eq. (53), the free energy of the comb polymer in these conditions is given by:

$$F \approx R^{\,2}/M + M^{\,2}\,(1 + z^{\,2}\,R_s^{\,3})\,/\,(H\,R^{\,2}) \tag{61}$$

Minimization of eq. (61) with respect to R provides the equilibrium configuration of the comb polymer of SCNPs under 2D-confinement ($R_s \ll H \ll R_s^{star}$):

$$R_{2D}^{combr} \approx M^{\,3/4}\,[(1 + z^{\,2}\,R_s^{\,3})\,/\,H\,]^{\,1/4} = M^{\,3/4}\,[\,(1 + z^{\,2}\,K^{\,-3/5}\,n^{\,6/5})\,/\,H\,]^{\,1/4} \tag{62}$$

4.4. Height of a brush of comb polymers of elastic single-chain nanoparticles anchored to a surface immersed in a good solvent

We consider here the case of a brush of comb polymers of SCNPs (each SCNP of size R_s) on a flat surface immersed in a good solvent in which the comb is anchored to the surface by one end of the main chain. Let us assume that the average distance between anchored combs is $d \to R_s$ and hence the grafting density is $\sigma = 1/d^2$. Accordingly, each comb of elastic SCNPs in the brush is confined to a volume proportional to $d^2\,R_a^{comb}$, where R_a^{comb} is the average brush height. From eq. (53), the free energy of a comb polymer of SCNPs in the brush can be expressed as:

$$F \approx R^{\,2}/M + M^{\,2}\,(1 + z^{\,2}\,R_s^{\,3})\,\sigma\,/\,R \tag{63}$$

Minimization of eq. (63) with respect to R gives the equilibrium height of the brush:

$$R_a^{comb} \approx M\,[\,(1 + z^{\,2}\,R_s^{\,3})\,\sigma\,]^{\,1/3} = M\,[\,(1 + z^{\,2}\,K^{\,-3/5}\,n^{\,6/5})\,\sigma\,]^{\,1/3} \tag{64}$$

Table 3 summarizes the scaling laws corresponding to comb polymers of SCNPs and the equivalent ones for combs of linear polymers.

5. Bottlebrush polymers of elastic single-chain nanoparticles

Upon increasing the grafting density, a comb polymer composed of SCNPs transforms into a brush polymer of SCNPs in which interactions between side SCNPs (that notably alter its size from R_s) become relevant

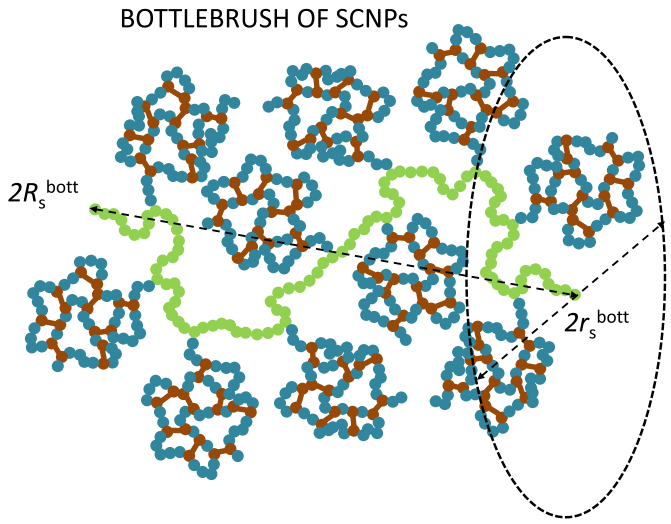

Fig. 9. Schematic illustration of a bottlebrush polymer composed of elastic single-chain nanoparticles in good solvent conditions in which interactions between side SCNPs are relevant for determining the local size (r_s^{bott}) and the global size (R_s^{bott}) of the bottlebrush.

for determining the local size (r_s^{bott}) and global dimension (R_s^{bott}) of the bottlebrush (see Fig. 9). Depending on the flexibility of the backbone (main chain) we can consider two limiting cases: i) rigid bottlebrush polymers of elastic SCNPs (*i.e.,* rigid backbone), and ii) flexible bottlebrush polymers of elastic SCNPs (*i.e.,* flexible main chain).

5.1. Thickness of rigid bottlebrushes of elastic single-chain nanoparticles in good solvent conditions at high dilution

This case is relevant for considering the layer thickness (r_s^{bott}) of a rigid cylinder of radius r_0 (*e.g.* nanotube, rigid helical chain) densely decorated with SCNPs in good solvent conditions at high dilution. We assume both the average distance between SCNPs attached to the cylinder (h) and r_0 are smaller compared to r_s^{bott} ($h, r_0 \ll r_s^{bott}$). As in the case of stars of SCNPs, we can combine the DC model [17] –adapted to cylindrical geometry [28]– with the ESN model [11] to obtain an expression for r_s^{bott}. In this case, from geometrical considerations, the blob size at a distance r from the nanotube center is:

$$\xi(r) \approx (r\ h)^{1/2} \tag{65}$$

so, the number of monomers per blob as a function of r is:

$$g(r) \approx K^{1/2}\ (r\ h)^{5/4} \tag{66}$$

The expansion parameter of the blobs and the segment concentration profile as a function of r become:

$$\alpha_b(r) \approx K^{-1/16}\ (r\ h)^{1/32} \tag{67}$$

and

$$\varphi(r) \approx K^{1/2}\ (r\ h)^{-1/4} \tag{68}$$

respectively. In this case, the blob size reaches the size of an ideal blob (*i.e.,* $\alpha_b(r) \approx 1$) at:

$$r_1 \approx K^2 / h \tag{69}$$

From eq. (68) we have: $\varphi(r_1) = 1$. Hence, from r_0 to r_1 we have a dense layer of blobs at the maximum density.

The layer thickness of the rigid bottlebrush of SCNPs –as obtained from $n = \int_0^{r_s^{bott}} g(r)\frac{dr}{\xi(r)}$ by assuming $r_0/r_s^{bott} \ll 1$– is:

Table 4
Layer Thickness of Rigid Bottlebrushes Composed of Elastic SCNPs *vs.* Rigid Bottlebrushes of LPs[a].

Conditions	Thickness	
	Rigid Bottlebrushes of SCNPs	Rigid Bottlebrushes of LPs
Good solvent, high dilution	$r_s^{bott} \approx h^{-3/7} K^{-2/7} n^{4/7}$	$r_s^{bott} \approx h^{-1/4} n^{3/4}$
Theta solvent, high dilution/ melt state	$r_m^{bott} \approx h^{-5/11} K^{-2/11} n^{6/11}$	$r_m^{bott} \approx h^{-1/3} n^{2/3}$

[a] h = Average distance between SCNPs attached to the cylindrical bottlebrush per unit length; K = SCNP elasticity parameter; n = number of monomers per SCNP.

$$r_s^{bott} \approx h^{-3/7} K^{-2/7} n^{4/7} \tag{70}$$

From eqs. (69) and (70), the ratio of the size of the core to the layer thickness is just:

$$r_1 / r_s^{bott} \approx h^{-4/7} K^{16/7} n^{-4/7} \tag{71}$$

The free energy per side SCNP calculated by assuming that each blob contribute with k_BT units to F_s^{bott} is:

$$F_s^{bott} \approx (r_s^{bott} / h)^{1/2} \approx h^{-5/7} K^{-1/7} n^{2/7} \tag{72}$$

5.2. Ideal thickness of rigid bottlebrushes of elastic single-chain nanoparticles

The ideal thickness of a rigid bottlebrush of elastic SCNPs, r_m^{bott}, corresponds to the case of negligible pairwise excluded-volume interactions [39]. Now, the blob size, the number of monomers per blob and the segment concentration profile as a function of r are given respectively by:

$$\xi_0(r) \approx (r\ h)^{1/2} \tag{73}$$

$$g(r) \approx K^{1/3}\ (r\ h)^{4/3} \tag{74}$$

$$\varphi(r) \approx K^{1/3}\ (r\ h)^{-1/6} \tag{75}$$

From eq. (75) the segment concentration profile becomes unity at $r_1 \approx K^2/h$, a result identical to that obtained for a rigid bottlebrush of elastic SCNPs in good solvent conditions (eq. (69)). From $n = \int_0^{r_m^{bott}} g(r)\frac{dr}{\xi(r)}$,

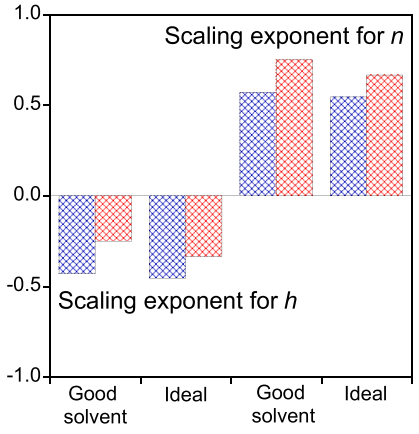

Fig. 10. Comparison of the scaling exponents for h and n (see Table 4) under different conditions corresponding to the layer thickness (r^{bott}) of rigid bottlebrush polymers composed of elastic SCNPs (blue grid bars) vs. rigid bottlebrushes of linear polymers (red grid bars). (For interpretation of the references to color in this figure legend, the reader is referred to the Web version of this article.)

we obtain an expression for the ideal layer thickness of a rigid bottlebrush of elastic SCNPs such as:

$$r_m^{bott} \approx h^{-5/11} K^{-2/11} n^{6/11} \quad (76)$$

The ratio of the size of the core to the layer thickness is:

$$r_1 / r_s^{bott} \approx h^{-6/11} K^{24/11} n^{-6/11} \quad (77)$$

In this case, the free energy per side SCNP becomes:

$$F_m^{bott} \approx (r_m^{bott} / h)^{1/2} = h^{-8/11} K^{-1/11} n^{3/11} \quad (78)$$

Table 4 summarizes the scaling laws corresponding to rigid bottlebrush polymers of elastic SCNPs and the equivalent ones for rigid bottlebrushes of linear polymers [44], whereas Fig. 10 shows a visual comparison of the scaling exponents for h and n in both cases.

5.3. Local structure and global size of flexible bottlebrush polymers of elastic single-chain nanoparticles in good solvent conditions at high dilution

In this case, crowding of the SCNPs grafts induces their extension in the radial direction and leads −additionally− to axial tension in the flexible backbone. We assume that both the bottlebrush backbone and the SCNPs pendants are in good solvent conditions. The local structure and global size of a flexible bottlebrush of elastic SCNPs can be analyzed following a coarse-graining approach [21,28,44,45]. First, at a length scale on the order of r_s^{bott} (Fig. 9) the bottlebrush is considered as a rigid bottlebrush with densely grafted SCNPs. Next, the size of a semiflexible chain of large blobs of size r_s^{bott} in good solvent conditions provides the global bottlebrush size, R_s^{bott}.

Local Bottlebrush Structure: The local bottlebrush structure is comprised of large blobs (so-called "superblobs" [28]) of size r_s^{bott} containing r_s^{bott}/h_0 side SCNPs, where h_0 is the equilibrium distance between SCNPs in the flexible backbone. The equilibrium stretching of the backbone at the r_s^{bott} scale is determined by a balance between the tension induced by the SCNP grafts and the restoring force arising from the conformational entropy of the backbone. Accordingly, the free energy of the backbone in the superblob can be written as:

$$F \approx h^{-5/7} K^{-1/7} n^{2/7} + h^{5/2} m^{-3/2} \quad (79)$$

where the first term takes into account the free energy per side SCNP in a rigid bottlebrush with densely grafted SCNPs (eq. (72)) and the second term corresponds to the Pincus free energy [46] to stretch the m monomers of the backbone involved at the scale of r_s^{bott}. Minimization of eq. (79) with respect to h gives the equilibrium value of the distance between SCNPs in the superblob, h_0, as a function of K, n and m:

$$h_0 \approx K^{-2/45} m^{7/15} n^{4/45} = K^{-2/45} m^{5/9} (n / m)^{4/45} \quad (80)$$

By combining eq. (80) with eq. (70) and eq. (72) we obtain, respectively:

$$r_s^{bott} \approx K^{-4/15} m^{-1/5} n^{8/15} = K^{-4/15} n^{1/3} (n / m)^{1/5} \quad (81)$$

$$F_s^{bott} \approx K^{-1/9} m^{-1/3} n^{2/9} = K^{-1/9} n^{-1/9} (n / m)^{1/3} \quad (82)$$

Global Bottlebrush Size: We assume that at large scale, the flexible bottlebrush of elastic SCNPs behaves as a flexible self-avoiding chain composed of $N_{sb} = (M/[m\,(r_s^{bott}/h_0)])$ superblobs [44] of size r_s^{bott}, such as:

$$R_s^{bott} \approx r_s^{bott} (N_{sb})^{3/5} = (r_s^{bott})^{2/5} (M\, h_0 / m)^{3/5} \quad (83)$$

Eq. (83) can be formally obtained by minimization of the following mean-field free energy expression:

$$F \approx R^2 / [(r_s^{bott})^2 N_{sb}] + [(r_s^{bott})^3 N_{sb}^2] / R^3 \quad (84)$$

We will return to eq. (84) below to estimate the size of a flexible bottlebrush of elastic SCNPs in good solvent conditions under confinement and the height of a planar brush composed of flexible bottlebrushes of elastic SCNPs tethered by their ends to the surface in the weakly overlapping regime.

From eqs. (80), (81) and (83) we obtain the scaling dependence of the overall dimension of the flexible bottlebrush of elastic SCNPs:

$$R_s^{bott} \approx M^{3/5} K^{-2/15} m^{-2/5} n^{4/15} = M^{3/5} K^{-2/15} n^{-2/15} (n / m)^{2/5} \quad (85)$$

Eq. (85) is valid at high grafting density such as crowding of the SCNPs grafts induces their extension in the radial direction and leads −additionally− to axial tension in the flexible backbone. The critical value of m for which the size of the SCNPs grafts remains unaltered (m_c) can be determined by equating eq. (81) to the size of an "unperturbed" SCNP in good solvent (eq. (4)). Accordingly, we obtain:

$$m_c \approx K^{-1/3} n^{2/3} \quad (86)$$

Exactly the same expression results by equating eq. (80) to the "unperturbed" distance of m backbone monomers in good solvent conditions ($\approx m^{3/5}$). Consequently, eq. (85) is valid for grafting densities higher than $z_c = 1/m_c \approx K^{1/3} n^{-2/3}$.

5.4. Local structure and global size of ideal flexible bottlebrush polymers of elastic single-chain nanoparticles

The above coarse-graining approach can be used to estimate the local structure (r_m^{bott}) and global size (R_m^{bott}) of an ideal flexible bottlebrush of elastic SCNPs.

Local Bottlebrush Structure: The equilibrium stretching of the backbone at the r_m^{bott} scale is now determined by a balance between the tension induced by the SCNP grafts and the restoring force arising from the conformational entropy of the backbone [39] according to:

$$F \approx h^{-8/11} K^{-1/11} n^{3/11} + h^2 m^{-1} \quad (87)$$

Minimization of eq. (87) with respect to h gives an expression for h_{0m} as a function of K, n and m:

$$h_{0m} \approx K^{-1/30} m^{11/30} n^{1/10} = K^{-1/30} m^{7/15} (n / m)^{1/10} \quad (88)$$

By combining eq. (88) with eq. (76) and eq. (78) we obtain, respectively:

$$r_m^{bott} \approx K^{-1/6} m^{-1/6} n^{1/2} = K^{-1/6} n^{1/3} (n / m)^{1/6} \quad (89)$$

$$F_m^{bott} \approx K^{-1/15} m^{-1/10} n^{1/5} = K^{-1/15} n^{1/10} (n / m)^{1/10} \quad (90)$$

Global Bottlebrush Size: At large scale, the ideal flexible bottlebrush of elastic SCNPs behaves as a flexible self-avoiding chain composed of $N_0 = (M/[m\,(r_m^{bott}/h_{0m})])$ superblobs of size r_m^{bott}, such as [28,44]:

$$R_m^{bott} \approx r_m^{bott} (N_0)^{3/5} = (r_m^{bott})^{2/5} (M\, h_{0m} / m)^{3/5} \quad (91)$$

From eqs. (88), (89) and (91) we obtain the scaling dependence of the overall dimension of the ideal flexible bottlebrush of elastic SCNPs:

$$R_m^{bott} \approx M^{3/5} K^{-13/150} m^{-67/150} n^{13/50} = M^{3/5} K^{-13/150} n^{-14/75} (n / m)^{67/150} \quad (92)$$

Following an analysis similar to that carried out to arrive at eq. (86) but using eqs. (88) and (89), it can be easily shown that eq. (92) is valid for grafting densities higher than:

$$z_c = 1/ m_c \approx K^{1/4} n^{-3/4} \quad (93)$$

5.5. Global size of flexible bottlebrush polymers of elastic single-chain nanoparticles in good solvent conditions under 1D and 2D confinement

1D-Confinement: Let us assume that a flexible bottlebrush of elastic SCNPs is confined in good solvent conditions in a cylindrical nanopore of

Table 5
Conformational Properties of Flexible Bottlebrush Polymers (High Grafting Density) Composed of Elastic SCNPs *vs.* Bottlebrushes of LPs[a].

Conditions	Size	
	Flexible Bottlebrushes of SCNPs	Bottlebrushes of LPs
Good solvent, high dilution	$r_s^{bott} \approx K^{-4/15} m^{-1/5} n^{8/15}$ $R_s^{bott} \approx M^{3/5} K^{-2/15} m^{-2/5} n^{4/15}$	$r_s^{bott} \approx m^{-3/25} n^{18/25}$ $R_s^{bott} \approx M^{3/5} m^{-9/25} n^{9/25}$
Ideal state	$r_m^{bott} \approx K^{-1/6} m^{-1/6} n^{1/2}$ $R_m^{bott} \approx M^{3/5} K^{-13/150} m^{-67/150} n^{13/50}$	$r_m^{bott} \approx m^{-1/8} n^{5/8}$ $R_m^{bott} \approx M^{3/5} m^{-17/40} n^{13/40}$
1D-confinement, good solvent	$R_{1D}^{bott} \approx M K^{-2/9} m^{-2/3} n^{4/9} D^{-2/3}$	$R_{1D}^{bott} \approx M m^{-3/5} n^{3/5} D^{-2/3}$
2D-confinement, good solvent	$R_{2D}^{bott} \approx M^{3/4} K^{-1/6} m^{-1/2} n^{1/3} H^{-1/4}$	$R_{2D}^{bott} \approx M^{3/4} m^{-9/20} n^{9/20} H^{-1/4}$
Brush, good solvent	$R_a^{bott} \approx M K^{-2/9} m^{-2/3} n^{4/9} \sigma^{1/3}$	$R_a^{bott} \approx M m^{-3/5} n^{3/5} \sigma^{1/3}$

[a] M = number of monomers in the comb main chain; K = SCNP elasticity parameter; m = inverse of the grafting density along the backbone; n = number of monomers per SCNP; D = nanopore diameter; H = nanoslit width; σ = grafting density of the brush.

diameter $r_s^{bott} \ll D \ll R_s^{bott}$. The volume occupied by the bottlebrush will be proportional to $D^2 R_{1D}^{bott}$, where R_{1D}^{bott} is the size along the channel axis. From eq. (84), the free energy of a flexible bottlebrush of elastic SCNPs under 1D-confinement can be expressed as:

$$F \approx R^2 / [(r_s^{bott})^2 N_{sb}] + [(r_s^{bott})^3 N_{sb}^2] / (D^2 R) \quad (94)$$

Minimization of eq. (94) with respect to R provides an expression for the equilibrium configuration of the bottlebrush under 1D-confinement ($r_s^{bott} \ll D \ll R_s^{bott}$):

$$R_{1D}^{bott} \approx (r_s^{bott})^{5/3} N_{sb} D^{-2/3} = M K^{-2/9} m^{-2/3} n^{4/9} D^{-2/3} \quad (95)$$

2D-Confinement: A flexible bottlebrush of SCNPs placed in a rectangular nanoslit of width $r_s^{bott} \ll H \ll R_s^{bott}$ will be confined to a volume proportional to $H(R_{2D}^{bott})^2$, where R_{2D}^{bott} is the lateral size of the SCNP in the slit. Hence, based on eq. (84), the free energy of the bottlebrush under 2D-confinement is given by:

$$F \approx R^2 / [(r_s^{bott})^2 N_{sb}] + [(r_s^{bott})^3 N_{sb}^2] / (H R^2) \quad (96)$$

Minimization of eq. (96) with respect to R provides the equilibrium configuration of the bottlebrush under 2D-confinement ($r_s^{bott} \ll H \ll R_s^{bott}$):

$$R_{2D}^{bott} \approx (r_s^{bott})^{5/4} (N_{sb})^{3/4} H^{-1/4} = M^{3/4} K^{-1/6} m^{-1/2} n^{1/3} H^{-1/4} \quad (97)$$

5.6. Height of a brush composed of flexible bottlebrush polymers of elastic single-chain nanoparticles anchored to a surface immersed in a good solvent

According to eq. (84), the free energy of a brush composed of flexible bottlebrush polymers of elastic SCNPs anchored −each bottlebrush polymer at one end− to a surface immersed in a good solvent can be expressed as:

$$F \approx R^2 / [(r_s^{bott})^2 N_{sb}] + [(r_s^{bott})^3 N_{sb}^2] \sigma / R \quad (98)$$

Where $\sigma = 1/d^2$ is the grafting density and d is the average distance between anchored bottlebrushes. Minimization of eq. (98) with respect to R gives the equilibrium height of the brush (weak overlapping regime):

$$R_a^{bott} \approx (r_s^{bott})^{5/3} N_{sb} \sigma^{1/3} = M K^{-2/9} m^{-2/3} n^{4/9} \sigma^{1/3} \quad (99)$$

Table 5 summarizes the scaling laws corresponding to flexible bottlebrush polymers of SCNPs and the equivalent ones for flexible bottlebrushes of linear polymers [28,44,45] in different conditions. The corresponding scaling exponents for m and n are compared in Figs. 11 and 12.

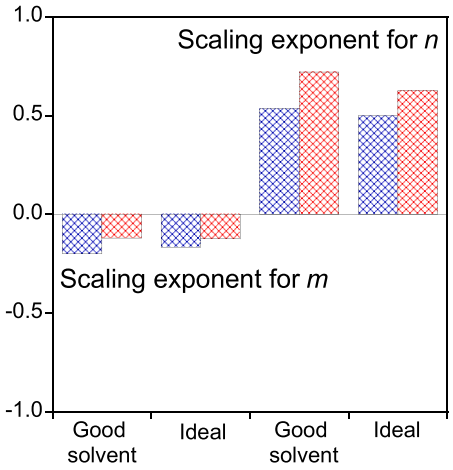

Fig. 11. Comparison of the scaling exponents for m and n (see Table 5) under different conditions corresponding to the local size (r^{bott}) of flexible bottlebrush polymers composed of elastic SCNPs (blue grid bars) vs. flexible bottlebrushes of linear polymers (red grid bars). (For interpretation of the references to color in this figure legend, the reader is referred to the Web version of this article.)

6. Discussion and conclusions

We have considered the integration of single-chain nanoparticles (SCNPs) into star, comb and bottlebrush topologies, investigated the conformational properties of the resulting superstructures under different relevant conditions (good solvent, ideal conformations, 1D-confinement in nanopores or flat surfaces, 2D-confinement in nanoslits) and compared the results to those of equivalent constructs of linear chains.

Firstly, to prepare the ground, we have summarized the main results of the elastic single-chain nanoparticle (ESN) model [11], as derived through a Flory free energy approximation, in several scenarios: i) a diluted solution (good solvent) composed of isolated SCNPs (size R_s), ii) in the ideal state (*i.e.,* the case of negligible pairwise excluded-volume interactions) (R_m), iii) in a good solvent under 1D- or 2D-confinement in nanopores or nanoslits, respectively (R_{1D}, R_{2D}) [12] and iv) for a densely array of elastic SCNPs anchored to a flat surface (R_a) [13]. The relevant model parameter is $K = Ax$, where A is a constant related to the elasticity of the SCNP composed of n monomers, and x is the fraction of reactive monomers involved in intra-chain cross-linking [11]. Based on selected experimental data, we have estimated (effective) values of A for PS-based SCNPs [37] (Fig. 2) and K for PMMA-based SCNPs [39] (section 2.2). We summarize the conformational properties of elastic SCNPs under different conditions compared to those of flexible linear polymers in Table 1. Interestingly, elastic SCNPs in a good solvent resemble randomly branched polymers with ideal connectivity in a theta-solvent or percolating clusters with screened excluded-volume interactions [30,31,34]. Overall, SCNPs show a reduction of the scaling exponent for n across all the relevant environments investigated: good solvent, melt, 1D-confinement both in nanopores and brushes on flat surfaces, and 2D-confinement in nanoslits (Fig. 3A). Notably, when compared to conventional linear chains, SCNP size can be additionally tuned by means of the parameter K related to the SCNP intra-chain cross-linking density, as illustrated in Fig. 13 for SCNPs and linear chains of identical n but different values of reactive functional groups, x, in good solvent conditions. We can estimate the lower value of x at which SCNPs behave as nanoparticles (within the ESN model approach) by equating the two

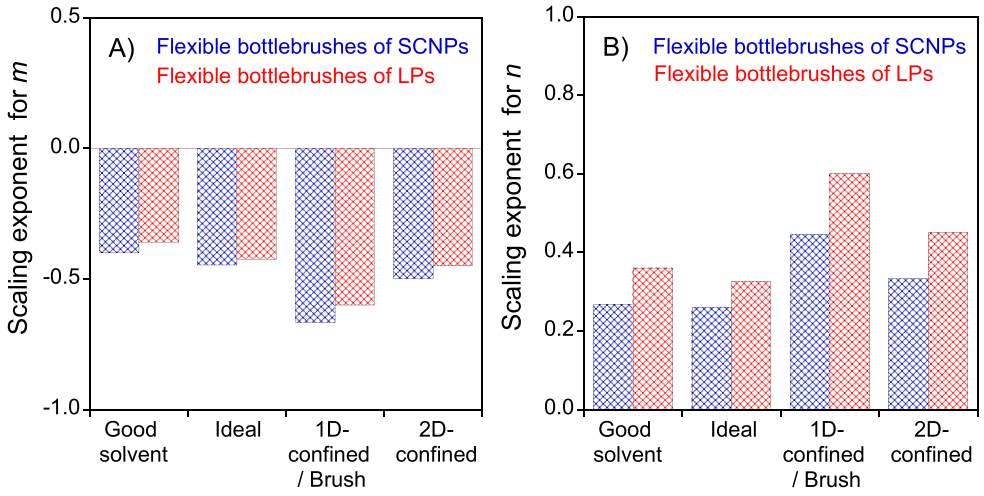

Fig. 12. Comparison of the scaling exponents for m (A) and n (B) corresponding to the global size (R^{bott}) under different conditions (see Table 5) of flexible bottlebrush polymers composed of elastic SCNPs (blue grid bars) vs. flexible bottlebrushes of linear polymers (red grid bars). (For interpretation of the references to color in this figure legend, the reader is referred to the Web version of this article.)

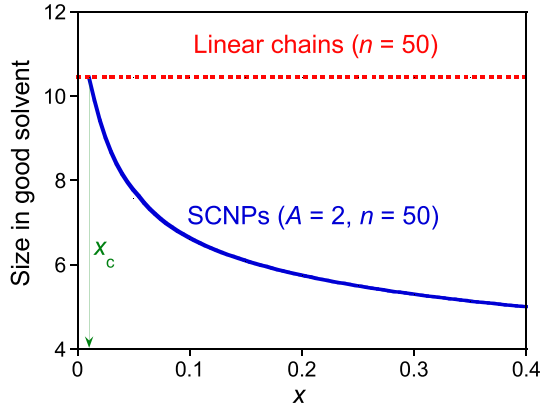

Fig. 13. Opposite to the case of linear chains of n monomers in good solvent (linear chain size: $R_l \approx n^{3/5}$, dashed red line), the size of SCNPs can be additionally tuned by means of the parameter $K = Ax$, where A is a constant related to the elasticity of the SCNP and x is the fraction of reactive monomers involved in intra-chain cross-linking (global SCNP size: $R_s \approx (A\,x)^{-1/5}\,n^{2/5}$; $x > x_c \approx (A\,n)^{-1}$). (For interpretation of the references to color in this figure legend, the reader is referred to the Web version of this article.)

terms of eq. (2) (*i.e.*, $K\,R^2 = R^2/R_0^2$). Accordingly, we obtain: $x_c \approx (A\,n)^{-1}$, that for typical values of A and n is very close to zero (see Fig. 13).

Secondly, we have investigated the conformational properties of star polymers composed of f SCNP arms through incorporation of the ESN model results (good solvent, ideal conditions) [11] within a scaling blob approach [17]. We have considered the case in which the size of the core of the star (r_c) is small referred to the global size of the star. Remarkably, the size of the core is found to be $r_c \approx K\,f^{1/2}$ both in good solvent and ideal conditions. The global size of a star of SCNPs in a good solvent is found to scale as $R_s^{star} \approx f^{3/10}\,R_s$, so the SCNPs in the star are elongated when compared to isolated SCNPs of size R_s. A mean-field free energy approximation, that fails to capture the effect of local fluctuations and inter-branch repulsion in the star of SCNPs, provides a scaling exponent of the dependence of R_s^{star} on f that is slightly lower (1/5). Interestingly, both approaches provide identical results if the excluded-volume contribution to the free energy in the mean-field approximation is increased by a factor $f^{1/2}$. Outside the core, the segment concentration profile decays with the distance from the center of the star as $r^{-1/2}$ (see Fig. 5). Within the scaling blob approach, the ideal size of a star of SCNPs is $R_m^{star} \approx f^{5/16}\,R_m$, which points to the stretching of the SCNP arms also in the case of negligible pairwise excluded-volume interactions. We summarize the conformational properties of star polymers composed of elastic SCNPs in several representative conditions in Table 2, that also include for comparison those of stars of linear polymers. Since we have neglected the classical R^2/R_0^2 contribution in eq. (2), we do not expect the expressions derived for stars of SCNPs to provide the equivalent expressions for linear chains in the limit of $x \to 0$. By incorporating this term, identical expressions to those reported in the literature result in the limit: $x \to 0$. Overall, the stars of SCNPs show an increase of the scaling exponent for f and a reduction of the scaling exponent for n when compared to stars of linear chains at all the relevant conditions investigated (see Fig. 6).

Thirdly, we have introduced a Flory free energy approximation to address the case of flexible comb polymers composed of elastic SCNPs in a variety of conditions. Depending on the grafting density ($z = 1/m$, m being the number of monomers between grafting points along the main chain) we distinguish between comb polymers of SCNPs if $z \ll 1$, and brush polymers of SCNPs if $z \to 1$. At low grafting density, we assume the size of a side SCNP is not disturbed by the presence of the other SCNPs pendants. For a comb polymer composed of SCNPs with M total number of monomers in the flexible backbone in good solvent conditions, we obtain the expected $R_s^{comb} \approx M^{3/5}$ scaling law when $z \to 0$ or $n \to 0$. Up to a critical grafting density given by $z_c \approx K^{1/3}\,n^{-2/3}$ the presence of the SCNPs pendants increases the equilibrium comb size according to $R_s^{comb} \approx M^{3/5}\,(1 + z^2\,R_s^3)^{1/5}$ even if the own size of the side SCNPs remains unaltered from R_s. Following a similar treatment, we obtain the ideal size of a comb polymer composed of SCNPs and the corresponding critical grafting density: $R_m^{comb} \approx M^{1/2}\,(1 + z^3\,R_m^3)^{1/8}$ and $z_c \approx K^{1/4}\,n^{-3/4}$, respectively. We compile the conformational properties of comb polymers of SCNPs under different relevant conditions vs. comb polymers of linear polymers in Table 3.

Fourthly, we have combined the elastic single-chain nanoparticle (ESN) model [11] with scaling blob theory [28,44] to investigate the conformational properties of rigid and flexible bottlebrushes composed of elastic SCNPs (high grafting density, $z > z_c$). The case of rigid bottlebrushes is relevant for determining the layer thickness of a rigid cylinder of radius r_0 (*e.g.* nanotube, rigid helical chain) densely decorated with SCNPs placed in good solvent (r_s^{bott}) or in the ideal state with negligible pairwise excluded-volume interactions (r_m^{bott}). We obtain $r_s^{bott} \approx h^{-3/7}\,K^{-2/7}\,n^{4/7}$ and $r_m^{bott} \approx h^{-5/11}\,K^{-2/11}\,n^{6/11}$, respectively, where h is the average distance between SCNPs attached to the rigid cylinder per unit length. When compared to the conformational properties of rigid

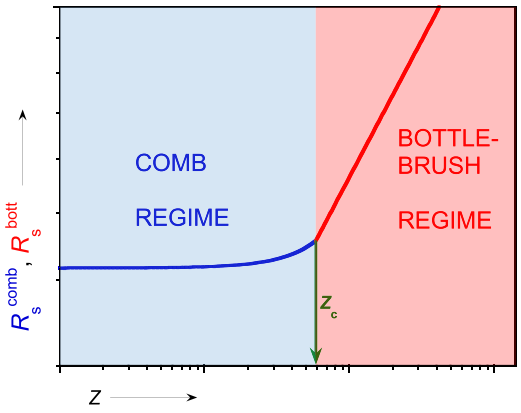

Fig. 14. Comb-to-bottlebrush transition of flexible polymer chains decorated with SCNPs (good solvent conditions) as a function of grafting density, z (log-log plot). The size of the side SCNPs remains unaltered until reaching a critical grafting density given by $z_c \approx K^{1/3}\, n^{-2/3}$. The comb and bottlebrush regimes correspond to $z < z_c$ (comb size: $R_s^{comb} \approx M^{3/5}\, [1 + z^2\, K^{-3/5}\, n^{6/5}]^{1/5}$) and $z > z_c$ (bottlebrush size: $R_s^{bott} \approx M^{3/5}\, K^{-2/15}\, z^{2/5}\, n^{4/15}$).

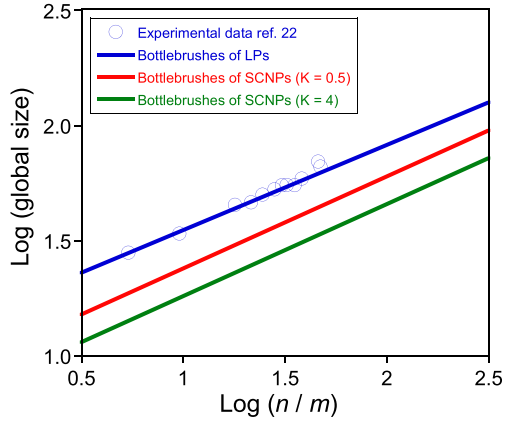

Fig. 15. Influence of the elasticity parameter K on the predicted global size of bottlebrushes of SCNPs vs. the size of bottlebrushes of linear polymers. Experimental data of well-defined PS-based bottlebrushes by Pan et al. [22] were selected to fix the numerical pre-factor used in the predictions (continuous lines).

bottlebrushes composed of linear chains [41] ($r_s^{bott} \approx h^{-1/4}\, n^{3/4}$, $r_m^{bott} \approx h^{-1/3}\, n^{2/3}$) rigid bottlebrushes of SCNPs display a reduction of the scaling exponent for h and n, both in good solvent and melt conditions (Fig. 10). Interestingly, the additional dependence of the layer thickness on K offers a possibility for tuning the layer thickness of rigid bottlebrushes of SCNPs *via* the degree of intramolecular cross-linking of the SCNPs. For the case of flexible bottlebrushes of SCNPs, we have adopted a coarse-graining approach [21,28,44] to investigate the local structure of rigid "superblobs" of size r_s^{bott} (good solvent) or r_m^{bott} (ideal conditions) and we have assumed that the size of a semiflexible chain composed of such superblobs provides the global bottlebrush size (R_s^{bott} or R_m^{bott}, respectively). Due to the high grafting density in a flexible bottlebrush of SCNPs, crowding of the SCNPs grafts induces their extension in the radial direction and leads −additionally− to axial tension in the flexible backbone. Within this approximation, for a flexible bottlebrush of SCNPs in good solvent we obtain: $r_s^{bott} \approx K^{-4/15}\, n^{1/3}\, (n/m)^{1/5}$ and $R_s^{bott} \approx M^{3/5}\, K^{-2/15}\, n^{-2/15}\, (n/m)^{2/5}$, whereas the classical result for an equivalent bottlebrush of linear polymers is [27,44]: $r_s^{bott} \approx n^{3/5}\, (n/m)^{3/25}$ and $R_s^{bott} \approx M^{3/5}\, (n/m)^{9/25}$. The latter scaling law prediction has been recently validated with a series of well-defined PS-based bottlebrushes by Pan et al. ($R_s^{bott} \approx (n/m)^{0.37 \pm 0.01}$) [22]. We summarize the conformational properties of flexible bottlebrushes of SCNPs in different conditions in Table 5 and illustrate the differences in scaling exponents between flexible bottlebrushes of SCNPs and linear polymers in Figs. 11 and 12. An illustrative example of the comb-to-bottlebrush transition in flexible polymer chains decorated with SCNPs as a function of grafting density is shown in Fig. 14. We provide in Fig. 15 a comparison of the size of flexible bottlebrushes of linear polymers in good solvent [22] vs. the predicted size of bottlebrushes of SCNPs as a function of the elasticity parameter K by assuming identical numerical pre-factor. Unfortunately, a direct comparison of the results obtained for bottlebrushes of SCNPs to those of dendronized polymers [47] is not possible since the size scaling of dendrimers in good solvent is expected to be [48] $R \sim n^{1/3}$ whereas, instead, the ESN model provides a size scaling $R \sim n^{2/5}$.

As a final remark, the degree of intra-chain cross-linking (which determines the value of K) arises as an additional parameter for controlling the local and global dimensions of a variety of superstructures based on elastic SCNPs under different relevant conditions (good solvent, ideal conformations, 1D- and 2D-confinement in nanopores and nanoslits, anchored to flat surfaces). This work provides useful guidelines for affording efficiently the construction of well-defined hierarchical superstructures based on SCNPs to broadening its potential utility in a number of applications (*e.g.,* catalysis, sensing, drug delivery).

CRediT authorship contribution statement

Davide Arena: Investigation, Writing – original draft. **Ester Verde-Sesto:** Investigation, Supervision, Writing – original draft. **José A. Pomposo:** Conceptualization, Supervision, Writing – review & editing.

Declaration of competing interest

The authors declare that they have no known competing financial interests or personal relationships that could have appeared to influence the work reported in this paper.

Data availability

Data will be made available on request.

Acknowledgement

Financial support by MCIN/AEI/10.13039/501100011033 and "ERDF – A way of making Europe" (PID2021-123438NB-I00), Eusko Jaurlaritza –Basque Government (IT1566-22) and Gipuzkoako Foru Aldundia, Programa Red Gipuzkoana de Ciencia, Tecnología e Innovación (2021-CIEN-000010-01) is gratefully acknowledged.

References

[1] F.J. Martin-Martinez, K. Jin, D. López Barreiro, M.J. Buehler, The rise of hierarchical nanostructured materials from renewable sources: learning from nature, ACS Nano 12 (2018) 7425–7433.
[2] G. Cai, P. Yan, L. Zhang, H.-C. Zhou, H.-L. Jiang, Metal-organic framework-based hierarchically porous materials: synthesis and applications, Chem. Rev. 121 (2021) 12278–12326.
[3] Z. Li, B. Cai, W. Yang, C.-L. Chen, Hierarchical nanomaterials assembled from peptoids and other sequence-defined synthetic polymers, Chem. Rev. 121 (2021) 14031–14087.
[4] A. Heuer-Jungemann, V. Linko, Engineering inorganic materials with DNA nanostructures, ACS Cent. Sci. 7 (2021) 1969–1979.
[5] J.A. Pomposo (Ed.), Single-Chain Polymer Nanoparticles: Synthesis, Characterization, Simulations, and Applications, Wiley-VCH, 2017.
[6] M.A.M. Alqarni, C. Waldron, G. Yilmaz, C.R. Becer, Synthetic routes to single chain polymer nanoparticles (SCNPs): current status and perspectives, Macromol. Rapid Commun. 42 (2021), 2100035.
[7] H. Frisch, B.T. Tuten, C. Barner-Kowollik, Macromolecular superstructures: a future beyond single chain nanoparticles, Isr. J. Chem. 60 (2020) 86–99.
[8] J.F. Chen, E.S. Garcia, S.C. Zimmerman, Intramolecularly cross-linked polymers: from structure to function with applications as artificial antibodies and artificial enzymes, Acc. Chem. Res. 53 (2020) 1244–1256.

[9] E. Verde-Sesto, A. Arbe, A.J. Moreno, D. Cangialosi, A. Alegría, J. Colmenero, J. A. Pomposo, Single-chain nanoparticles: opportunities provided by internal and external confinement, Mater. Horiz. 7 (2020) 2292–2313.
[10] R. Chen, E.B. Berda, 100th anniversary of macromolecular science viewpoint: Re-examining single-chain nanoparticles, ACS Macro Lett. 9 (2020) 1836–1843.
[11] J. De-La-Cuesta, E. González, A.J. Moreno, A. Arbe, J. Colmenero, J.A. Pomposo, Size of elastic single-chain nanoparticles in solution and on surfaces, Macromolecules 50 (2017) 6323–6331.
[12] J.A. Pomposo, J. Rubio-Cervilla, E. González, A.J. Moreno, A. Arbe, J. Colmenero, Ultrafiltration of single-chain polymer nanoparticles through nanopores and nanoslits, Polymer 148 (2018) 61–67.
[13] I. Asenjo-Sanz, A.J. Moreno, A. Arbe, J. Colmenero, J.A. Pomposo, Brushes of elastic single-chain nanoparticles on flat surfaces, Polymer 169 (2019) 207–214.
[14] A.D. Kazakov, V.M. Prokacheva, F. Uhlik, P. Kosovan, F.A.M. Leermakers, Computer modeling of polymer stars in variable solvent conditions: a comparison of MD simulations, self-consistent field (SCF) modeling and novel hybrid Monte Carlo SCF approach, Soft Matter 17 (2021) 580–591.
[15] J. Paturej, A. Milchev, S.A. Egorov, K. Binder, Star polymers confined in a nanoslit: a simulation test of scaling and self-consistent field theories, Soft Matter 9 (2013) 10522–10531.
[16] E.B. Zhulina, T.M. Birshtein, O.V. Borisov, Curved polymer and polyelectrolyte brushes beyond the Daoud-Cotton model, Eur. Phys. J. E: Soft Matter Biol. Phys. 20 (2006) 243–256.
[17] M. Daoud, J.P. Cotton, Star shaped polymers: a model for the conformation and its concentration dependence, J. Phys. (Paris) 43 (1982) 531–538.
[18] M. Abbasi, L. Faust, K. Riazi, M. Wilhelm, Linear and extensional rheology of model branched polystyrenes: from loosely grafted combs to bottlebrushes, Macromolecules 50 (2017) 5964–5977.
[19] R. Verduzco, X.Y. Li, S.L. Pesek, G.E. Stein, Structure, function, self-assembly, and applications of bottlebrush copolymers, Chem. Soc. Rev. 44 (2015) 2405–2420.
[20] D. Chatterjee, T.A. Vilgis, Scaling laws of bottle-brush polymers in dilute solutions, Macromol. Theory Simul. 25 (2016) 518–523.
[21] J. Paturej, T. Kreera, Hierarchical excluded volume screening in solutions of bottlebrush polymers, Soft Matter 13 (2017) 8534–8541.
[22] X. Pan, M. Ding, L. Li, Experimental validation on average conformation of a comblike polystyrene library in dilute solutions: universal scaling laws and abnormal SEC elution behavior, Macromolecules 54 (2021) 11019–11031.
[23] W.F.M. Daniel, J. Burdynska, M. Vatankhah-Varnoosfaderani, K. Matyjaszewski, J. Paturej, M. Rubinstein, A.V. Dobrynin, S.S. Sheiko, Solvent-free, supersoft and superelastic bottlebrush melts and networks, Nat. Mater. 15 (2015) 183–189.
[24] Z. Zhang, J.M.Y. Carrillo, S.K. Ahn, B. Wu, K.L. Hong, G.S. Smith, C. Do, Atomistic structure of bottlebrush polymers: simulations and neutron scattering studies, Macromolecules 47 (2014) 5808–5814.
[25] P.E. Theodorakis, H.P. Hsu, W. Paul, K. Binder, Computer simulation of bottle-brush polymers with flexible backbone: good solvent versus theta solvent conditions, J. Chem. Phys. 135 (2011), 164903.
[26] S. Rathgeber, T. Pakula, A. Wilk, K. Matyjaszewski, H.I. Lee, K.L. Beers, Bottle-brush macromolecules in solution: comparison between results obtained from scattering experiments and computer simulations, Polymer 47 (2006) 7318–7327.
[27] Y. Rouault, O.V. Borisov, Comb-branched polymers: Monte Carlo simulation and scaling, Macromolecules 29 (1996) 2605–2611.
[28] T.M. Birshtein, O.V. Borisov, Y.B. Zhulina, A.R. Khokhlov, T.A. Yurasova, Conformations of comb-like macromolecules, Polym. Sci. 29 (1987) 1293–1300.
[29] G.H. Fredrickson, Surfactant-induced lyotropic behavior of flexible polymer solutions, Macromolecules 26 (1993) 2825–2831.
[30] A. Chremos, J.F. Douglas, A comparative study of thermodynamic, conformational and structural properties of bottlebrush with star and ring polymer melts, J. Chem. Phys. 149 (2018), 044904.
[31] R. Everaers, A.Y. Grosberg, M. Rubinstein, A. Rosa, Flory theory of randomly branched polymers, Soft Matter 13 (2017) 1223–1234.
[32] G. Parisi, N. Sourlas, Critical behavior of branched polymers and the lee-yang edge singularity, Phys. Rev. Lett. 46 (1981) 871–874.
[33] A.Y. Grosberg, Annealed lattice animal model and Flory theory for the melt of non-concatenated rings: towards the physics of crumpling, Soft Matter 10 (2014) 560–565.
[34] J.F. Douglas, Swelling and growth of polymers, membranes, and sponges, Phys. Rev. E 54 (1996) 2677–2689.
[35] E.B. Zhulina, S.S. Sheiko, O.V. Borisov, Solution and melts of barbwire bottlebrushes: hierarchical structure and scale-dependent elasticity, Macromolecules 52 (2019) 1671–1684.
[36] T.A. Vilgis, Crosslinked polymer chains with excluded volume: a new class of branched polymers? Macromol. Theory Simul. 7 (1998) 59–63.
[37] H. Rabbel, P. Breier, J.-U. Sommer, Swelling behavior of single-chain polymer nanoparticles: theory and simulation, Macromolecules 50 (2017) 7410–7418.
[38] J.A. Pomposo, A.J. Moreno, A. Arbe, J. Colmenero, Local domain size in single-chain polymer nanoparticles, ACS Omega 3 (2018) 8648–8654.
[39] M. Rubinstein, R.H. Colby, Polymer Physics, Oxford University Press, Inc., New York, 2003.
[40] E. Harth, B. Van Horn, V.Y. Lee, D.S. Germack, C.P. Gonzales, R.D. Miller, C. J. Hawker, A facile approach to architecturally defined nanoparticles via intramolecular chain collapse, J. Am. Chem. Soc. 124 (2002) 8653–8660.
[41] A.J. Moreno, F. Lo Verso, A. Arbe, J.A. Pomposo, J. Colmenero, Concentrated solutions of single-chain nanoparticles: a simple model for intrinsically disordered proteins under crowding conditions, J. Phys. Chem. Lett. 7 (2016) 838–844.
[42] M. González-Burgos, A. Arbe, A.J. Moreno, J.A. Pomposo, A. Radulescu, J. Colmenero, Crowding the environment of single-chain nanoparticles: a combined study by SANS and simulations, Macromolecules 51 (2018) 1573–1585.
[43] T. Sakaue, F. Brochard-Wyart, Nanopore-based characterization of branched polymers, ACS Macro Lett. 3 (2014) 194–197.
[44] O.V. Borisov, in: K. Matyjaszewski, M. Möller (Eds.), *Static And Dynamic Properties* in *Polymer Science: A Comprehensive Reference*, Elsevier, 2012.
[45] E.B. Zhulina, T.A. Vilgis, Scaling theory of planar brushes formed by branched polymers, Macromolecules 28 (1995) 1008–1015.
[46] P. Pincus, Excluded volume effects and stretched polymer chains, Macromolecules 9 (1976) 386–388.
[47] A.D. Schlüter, J.P. Rabe, Dendronized Polymers: Synthesis, Characterization, Assembly and Manipulation, third ed., Wiley, New York, 2001.
[48] M. Ballauff, C.N. Likos, Dendrimers in solution: insight from theory and simulation, Angew. Chem. Int. Ed. 43 (2004) 2998–3020.